Macromolecular Research

Article

DOI 10.1007/s13233-019-7109-1

www.springer.com/13233 pISSN 1598-5032 eISSN 2092-7673

Morphology and Mechanical Properties of Polyketone/Polycarbonate Blends Compatibilized with SEBS and Polyamide

Ikseong Jeon
Mingyu Lee
Seung Woo Lee
Jae Young Jho*

School of Chemical and Biological Engineering, Seoul National University, Seoul 08826, South Korea

Received December 24, 2018 / Revised January 9, 2019 / Accepted January 10, 2019

Abstract: To enhance the impact strength of polyketone (PK) without the decrease in its stiffness, PK was blended with polycarbonate (PC). For the effective toughening of PK/PC blends, polyamide 6 (PA6) and mixtures of unmodified poly[styrene-*b*-(ethylene-*co*-butylene)-*b*-styrene] (unSEBS) and maleic anhydride (MA)-grafted SEBS (SEBS-*g*-MA) were added to the blends as compatibilizers. Examining the fracture surface, it was observed that, by varying the SEBS-*g*-MA/unSEBS ratio in the compatibilizer, the phase morphology and interphase structure were changed. While PK/PC/SEBS-*g*-MA/PA6 blend had completely encapsulated PC domains, PK/PC/(SEBS-*g*-MA/unSEBS)/PA6 blends showed a morphology in which the PC was incompletely encapsulated by SEBS. Morphological differences, such as complete or incomplete PC encapsulation, led to differences in the impact strength. The impact strength of the blends with incomplete encapsulation of PC was higher than that with complete encapsulation of PC. Through the investigation of fracture behaviors, it was confirmed that the impact strength of PK/PC/(SEBS-*g*-MA/unSEBS)/PA6 was enhanced due to debonding around the incompletely encapsulated PC particles and matrix shear yielding.

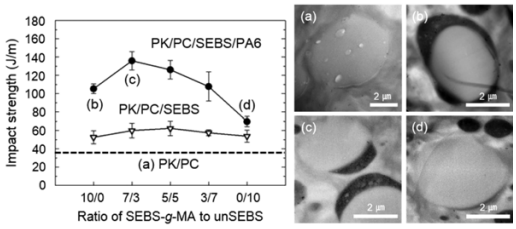

Keywords: polyketone, polycarbonate, compatibilizer, impact strength, phase morphology.

1. Introduction

Aliphatic polyketone (PK) is a terpolymer composed of carbon monoxide, ethylene, and a small amount of propylene. Compared with other engineering plastics, PK has better barrier property, abrasion resistance, and chemical resistance.[1-4] In particular, PK has received considerable attention due to its superior barrier properties over other packaging materials such as polyesters. While the mechanical properties including tensile strength of PK are comparable to those of polyamide 6 (PA6), the impact strength is lower than that of tough polymers like polycarbonate (PC) or poly(acrylonitrile-butadiene-styrene) (ABS). The impact strength of PK needs to be improved to be used in a wide range of engineering or packaging applications.

To enhance the impact strength of PK, blending with other polymers including elastomers and thermoplastics has been attempted. As the examples of the elastomers blended with PK, maleic anhydride (MA)-grafted ethylene-octene rubber (mEOR), core-shell rubber (CSR), and ethylene/methacrylic acid copolymer have been reported. Blending elastomers with PK effectively enhanced the impact strength of PK, but had the problem of reducing the modulus and tensile strength.[5-7] As an alternative to the toughening of PK with elastomers, PK blended with thermoplastics has been proposed to obtain an enhanced impact strength without a reduction in the inherent stiffness. PC and some polyamides (PAs) such as PA6, polyamide 66 (PA66), and amorphous polyamide have been blended with PK.[8-11] In the PK/PA66 blends with a small amount of ethylene/methacrylic acid copolymer, enhanced impact strength and yield strength were observed. The PK/PA6 blends showed significant improvement in the impact strength under wet conditions, but showed only a slightly enhanced impact strength in dry conditions. An improved impact strength and tensile strength were observed in PK/PC blends containing PA-PC graft copolymer as a compatibilizer. When 50 wt% of PC was blended with PK, the impact strength of the blend was decreased because of poor compatibility. However, by adding 20 wt% of the PA-PC copolymer, the impact strength was enhanced by 46% compared to that of PK. This means that the degree of improvement in the impact strength of PK blended with thermoplastics is strongly influenced by its compatibility.

The impact strength of PK blends depends on the phase morphology as well as the compatibility.[12-14] The incorporation of additional blend components is a common way to change the phase morphology and improve the compatibility of the blends.[15,16] Particularly, when a component with a reactive functional group is added, the morphology is remarkably changed due to a chemical reaction occurring between the components, which affects the toughness and toughening mechanisms.[17] In a study of PK blended with mEOR and PA6, it was found that the impact strength of the blend was effectively enhanced by the formation of the morphology where mEOR particles were encapsulated by PA6.[5]

In the present study, PK was blended with PC for thermoplastic toughening. PC is a thermoplastic polymer suitable for

Acknowledgments: This work was supported by a grant from the Fundamental R&D Program for Technology of World Premier Materials funded by the Ministry of Trade, Industry, and Energy, Republic of Korea. This work was also supported by the Institute of Chemical Processes (ICP) at Seoul National University.

***Corresponding Author:** Jae Young Jho (jyjho@snu.ac.kr)

toughening due to its high impact strength and stiffness. To improve the compatibility of PK/PC blends, PA6 and poly[styrene-*b*-(ethylene-*co*-butylene)-*b*-styrene] (SEBS) were added to the blends. To modulate the phase morphology, two types of SEBS were used; unmodified SEBS (unSEBS) and MA-grafted SEBS (SEBS-*g*-MA). It has been known that PA6 is partially compatible with PK due to hydrogen bonding and can also react with the MA groups of SEBS-*g*-MA during melt blending.[9,18,19] In addition, SEBS-*g*-MA has been used in PA6/PC blends as a reactive compatibilizer.[16,20] Based on the above facts, the addition of PA6 and SEBS-*g*-MA was expected to improve the compatibility between PK and PC and to induce morphological changes. The different phase morphologies of the blends with varying ratios of SEBS-*g*-MA/unSEBS were investigated in detail through microscopic analysis. Through the investigation of impact-fracture behaviors, we discuss the toughening mechanisms dependent on the phase morphology of the blends.

2. Experimental

2.1. Materials

PK pellet with a melt flow index of 60 g/10 min (240 °C/2.16 kg) and PA6 pellet were supplied by Hyosung under the trade name of M330A and 1011BRT. PC pellet with a melt flow index of 15 g/10 min (300 °C/1.2 kg) was obtained from Lotte Chemical under the trade name of PC-1150. unSEBS and SEBS-*g*-MA were purchased from Kraton under the trade name of G1652 and FG1901G. All polymers were dried at 60 °C for 24 h in a vacuum oven to remove absorbed water before processing.

2.2. Preparation of blends

PK/PC blends containing PA6 and mixtures of unSEBS and SEBS-*g*-MA were prepared by using a co-rotating twin screw extruder (BA-19, Bautek, Korea) with temperature profiles of 260-270 °C from hopper to die at a screw rotating speed of 200 rpm. After extrusion, the blends were water-cooled, pelletized, and dried at 60 °C.

The compositions of the PK/PC blends are shown in Table 1. The weight fraction of PK/PC was held at 80/20 (wt%). Total amount of the SEBS-*g*-MA/unSEBS mixture was held constant at 10 phr (10 g against 100 g of PK/PC), while the amount of PA was held at 5 phr. The ratio of SEBS-*g*-MA and unSEBS was varied from 10/0 to 0/10. The blends were coded with letters and numbers. The letters K, C, S, and A refer to PK, PC, SEBS, and PA6, respectively. The number after the letter SA or S refers to the SEBS-*g*-MA/unSEBS ratio.

Table 1. Compositions of the PK/PC blends

Code	PK (wt%)	PC (wt%)	SEBS-*g*-MA (phr)	unSEBS (phr)	PA6 (phr)
KC	80	20	-	-	-
SA10/0	80	20	10	0	5
SA7/3	80	20	7	3	5
SA5/5	80	20	5	5	5
SA3/7	80	20	3	7	5
SA0/10	80	20	0	10	5
S10/0	80	20	10	0	-
S7/3	80	20	7	3	-
S5/5	80	20	5	5	-
S3/7	80	20	3	7	-
S0/10	80	20	0	10	-

2.3. Characterization of blends

The morphology of the blends was examined with a field emission scanning electron microscope (SEM, JEOL, JSM-6701F). To observe the particle size and phase morphology, the PC and PA6 phases were etched with chloroform and formic acid, respectively. The fracture surface was obtained by breaking the specimen after immersion in liquid nitrogen for 5 min. For the transmission electron microscopy (TEM, JEOL, JEM-2100F) studies, specimens were prepared by cryo-microtoming at -100 °C, followed by transferring onto carbon-coated Cu grids. Prepared specimens were stained with the vapors of ruthenium oxide (RuO_4, 0.5 wt% aqueous solution) for the SEBS and PA6 phases. The Fourier transform infrared (FT-IR) spectra of the blends were recorded using a FT-IR spectrometer (Thermo Scientific, Nicolet 6700) in a range from 3500 to 650 cm^{-1}.

The specimens for the tensile and impact tests were prepared using an injection-molding machine (Boy 12A, Boy Machines). The tensile properties were measured using a universal testing machine (UTM, LR10K, Lloyds Instruments) with a cross-head speed of 10 mm/min according to the ASTM D-638 Type V method, which is for specimens of 63.5×3.18×3.2 mm^3 in dimension. The notched Izod impact strength was measured at 25 °C using an impact tester (Tinius Olsen Model 92T) in accordance with ASTM D-256. The Izod impact test specimens with dimensions of 63.5×12.7×3.2 mm^3 were notched by the Tinius Olsen Model 899 specimen notcher. For investigation of the fracture behavior, the double-notch four-point-bend (DN-4PB) test was conducted using a rectangular bar of 63.5×12.7×3.2 mm^3 in dimension with two notches. The rectangular bar was first notched with a notch cutter to a depth of 2.5 mm, and the notch was further sharpened by opening a crack with a razor blade cooled in liquid nitrogen. During the DN-4PB test, one crack was broken while the other was sub-critically damaged. For the transmitted light optical microscopy (TOM) investigation of the sub-critically damaged zone near the crack tip, a thin section of the DN-4PB specimen including the damage zone was obtained by polishing. The damage zone was examined using an optical microscope (Leitz Laborlux 12 POL S, Leica).

3. Results and discussion

3.1. Morphology

Because the morphology of the blends affects the toughness and toughening mechanism, we observed the morphology through microscopic analysis. Figure 1 shows the SEM images of the cryofracture surfaces of KC, SA10/0, and SA5/5 with the PA6 phase removed, and the TEM image of SA5/5 stained with RuO_4. For

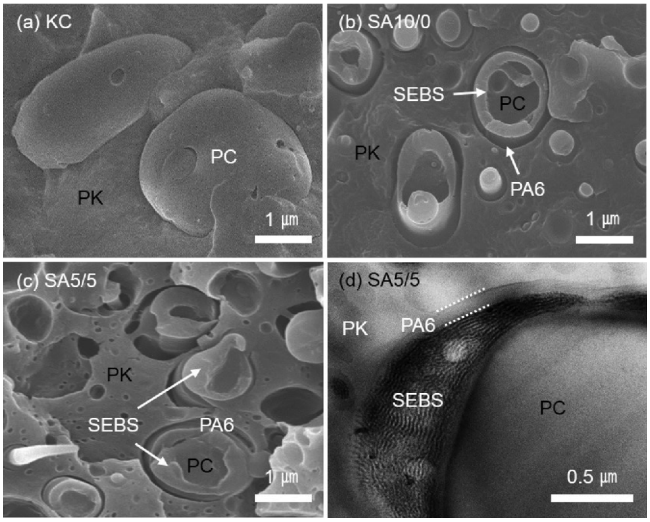

Figure 1. SEM micrographs of the cryofracture surfaces of (a) KC, (b) SA10/0, and (c) SA5/5 with the PA6 phase removed and TEM micrograph of (d) SA5/5 stained with RuO_4.

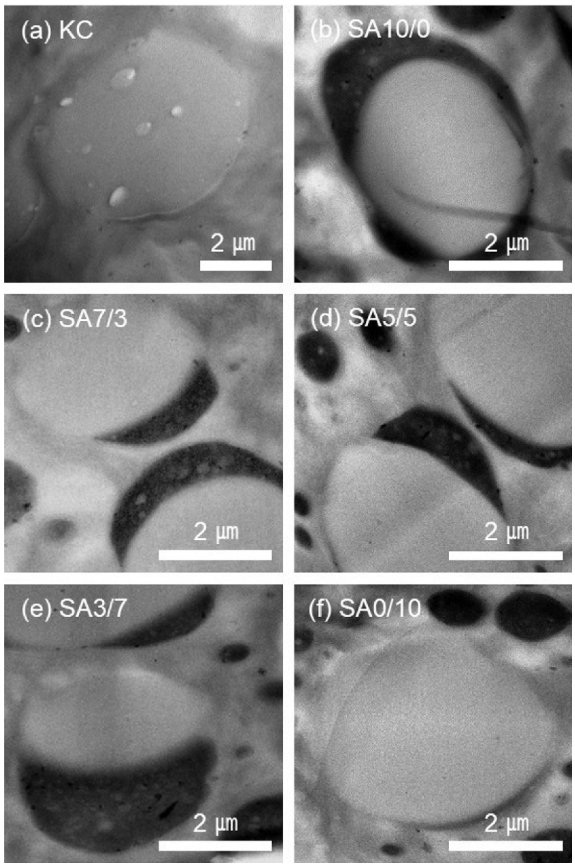

Figure 2. TEM micrographs showing the phase morphology of the PK/PC blends with various SEBS-*g*-MA/unSEBS ratios: (a) KC, (b) SA10/0, (c) SA7/3, (d) SA5/5, (e) SA3/7, and (f) SA0/10.

the SA10/0 and SA5/5 blends, a hierarchical ordering of PK/PA6/SEBS/PC was observed. The extracted PA6 layer was located between the SEBS and PK matrix while the PC domain was surrounded by SEBS. The PC particle size of SA10/0 and SA5/5 was smaller than that of KC, which indicates that the interfacial tension was reduced due to the encapsulation. The results of the TEM observation showed the morphology of SA5/5 clearly (Figure 1(d)). In the image, the SEBS phase strongly stained by RuO_4 is dark grey, and the weakly stained PA6 phase is light grey. SA5/5 exhibited a formation where the SEBS and PC were stuck together. It was also shown that the acorn-shaped domain composed of SEBS and PC was surrounded by a thin light grey PA6 layer.

The morphology changes of the PK/PC/SEBS/PA6 blends induced by varying the ratio of SEBS-*g*-MA to unSEBS are shown in Figure 2. For SA10/0, there was a dark grey layer between the PC and the PK. The complete encapsulation of PC was caused by a grafting reaction between the SEBS-*g*-MA and amine groups of PA6. It was difficult to determine the value of the interfacial tension between PA6 and SEBS, but it was certain that the reaction could reduce the interfacial tension between the two phases.[21] The decrease of the interfacial tension between SEBS and PA6, when the other interfacial tensions between the components were unchanged, enabled the encapsulation of the PC particles by placing SEBS at the interface of the PA6 and PC. Because some of the SEBS-*g*-MA were replaced by unSEBS, the encapsulation of PC by SEBS became incomplete. The incomplete encapsulation was observed in all PK/PC/(SEBS-*g*-MA/unSEBS)/PA6 blends. The morphological change from complete PC encapsulation to incomplete PC encapsulation was due to the increased interfacial tension between the SEBS and PA6 as the SEBS-*g*-MA content was decreased.[13] For SA0/10, which is an unreactive system, it was found that unSEBS and PC were separately dispersed in the PK matrix. Even in S0/10 where PA6 was absent, unSEBS formed isolated domains in the matrix (Figure S1 in the supporting information).

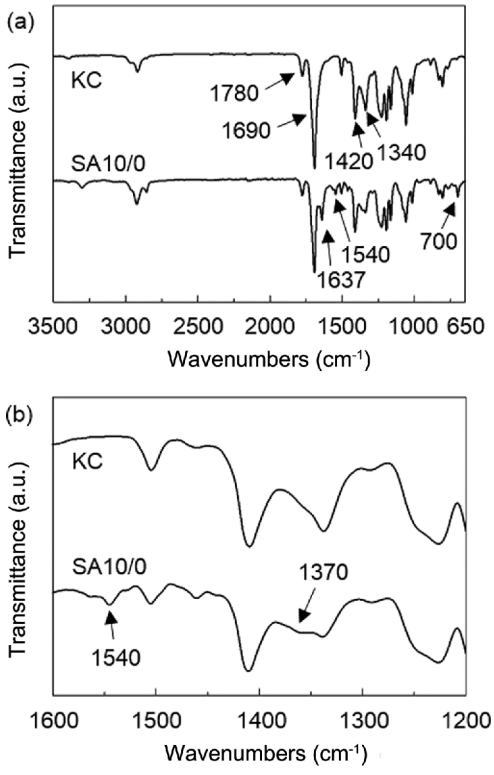

Figure 3. FT-IR spectra of KC and SA10/0. (a) 3500-650 cm^{-1} region; (b) magnified spectra of the 1600-1200 cm^{-1} region.

3.2. Reactive compatibilization

To identify the chemical reaction that occurred during melt blending, FT-IR analysis for PK/PC blends was conducted (Figure 3). In the spectrum of the KC, the peaks at 1780 and 1690 cm^{-1} were assigned to the C=O stretching of the carbonate groups and the C=O stretching of the PK. The C-H bending of the methylene and methyl groups of PK appeared at 1420 and 1340 cm^{-1}.[22,23] The C=O stretching of the aliphatic ketone was reported to be present at 1715 cm^{-1}, but the C=O stretching of PK appeared at 1690 cm^{-1}, which was due to the intra- and intermolecular dipole-dipole interaction between the carbonyl groups.[24] With the addition of PA6 and SEBS-*g*-MA, the spectrum of SA10/0 exhibited new characteristic peaks at 1637, 1540, and 700 cm^{-1} due to the C=O stretching of PA6, the C-N stretching vibration of PA6, and the aromatic C-H bending of the styrene unit of SEBS, respectively.[25] In Figure 3(b), which is a magnified view of the SA10/0 spectrum, the peak at 1370 cm^{-1} was due to the C-N stretching vibration of the imide groups which were formed by the reaction of MA with the amine of PA6.[24,26]

3.3. Mechanical properties

The results of the tensile and Izod impact tests are summarized in Figure 4. The PK/PC, PK/PC/SEBS, and PK/PC/SEBS/PA6 blends showed different fracture behaviors in the tensile tests. PK/PC prematurely failed at an elongation less than 20% without yielding while PK/PC/SEBS was fractured during necking propagation. PK/PC/SEBS/PA6 exhibited a drastic increase in the elongation at break up to 205% with complete necking. In Figure 4((a)-(c)), Young's modulus, tensile strength, and elongation at break of the blends are plotted as a function of the ratio of SEBS-*g*-MA to unSEBS. The Young's modulus of PK/PC/SEBS and PK/PC/SEBS/PA6 were lower than that of the PK/PC due to the addition of SEBS, but still similar to that of PK. The tensile strength of PK/PC/SEBS was slightly lower than that of PK/PC. The interfacial adhesion between the PC and PK matrix was improved by PA6 and SEBS added together in the blend, resulting in an increase in tensile strength. Elongation at break was strongly affected by the addition of SEBS and PA6 as well as the SEBS-*g*-MA/unSEBS ratio. PK/PC/SEBS/PA6 showed a significantly higher elongation at break than that of PK/PC/SEBS. The enhancement of the elongation at break was attributed to well-dispersed PC particles and a strong interfacial adhesion between components.[27] The PK/PC/(SEBS-*g*-MA/unSEBS)/PA6 blends (SA7/3, SA5/5, SA3/7) exhibited a higher elongation at break than the PK/PC/SEBS-*g*-MA/PA6 blend (SA10/0). The difference in elongation between these blends was attributed to the phase morphology and void generation during tensile deformation. As confirmed by the morphology observation, incomplete encapsulation of PC was induced by the addition of the SEBS-*g*-MA/unSEBS mixture. Due to the incomplete encapsulation, debonding occurred at the PC/PA6 interface where SEBS was not placed. Subsequently, the debonding developed into voids during the post-yield elongation. It was thought that the tensile stress was relieved effectively due to the void generation accompanied by deformation of SEBS.[28] For SA10/0, the PC particles were completely encapsulated by SEBS. Due to the complete encapsulation, the debonding at the interface occurred at a relatively later stage of the strain. However, it was considered that the fracture occurred immediately after the generation of debonding. In the case of SA0/10, the elongation at break was not greatly enhanced

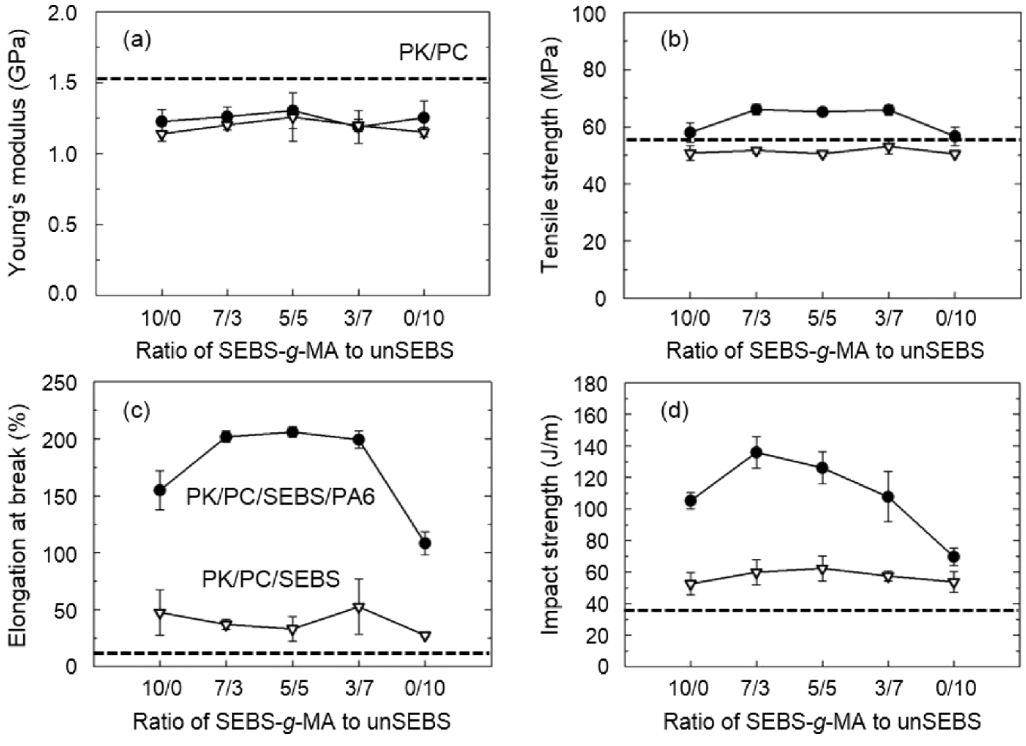

Figure 4. (a) Young's modulus, (b) tensile strength, (c) elongation at break, and (d) impact strength of the blends as a function of the ratio of SEBS-*g*-MA to unSEBS: ▽ PK/PC/SEBS, ● PK/PC/SEBS/PA6, and (---) PK/PC.

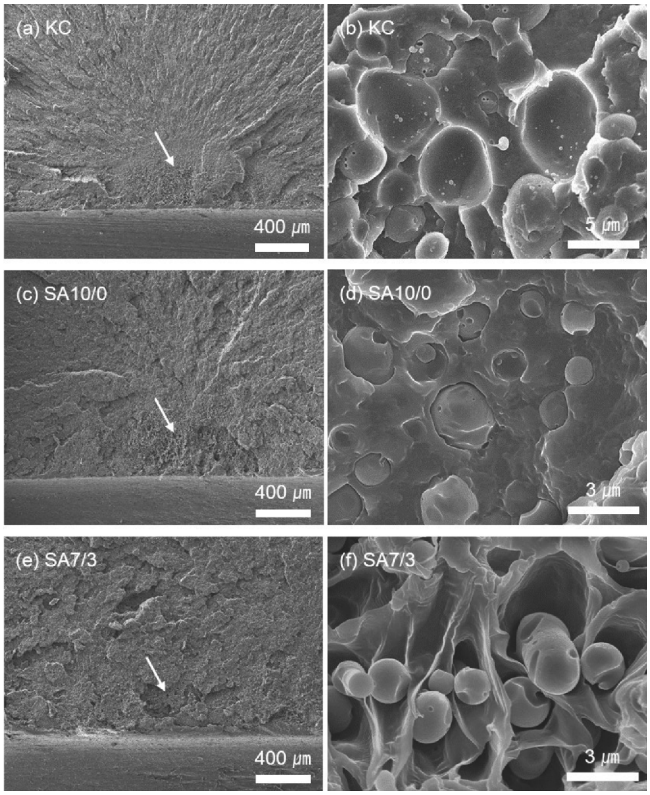

Figure 5. SEM images of impact-fracture surfaces of (a) KC, (c) SA10/0, and (e) SA7/3. (b), (d), and (f) show the magnified slow-crack-growth regions (indicated by the arrows) of (a), (c), and (e), respectively. The crack propagated from bottom to top.

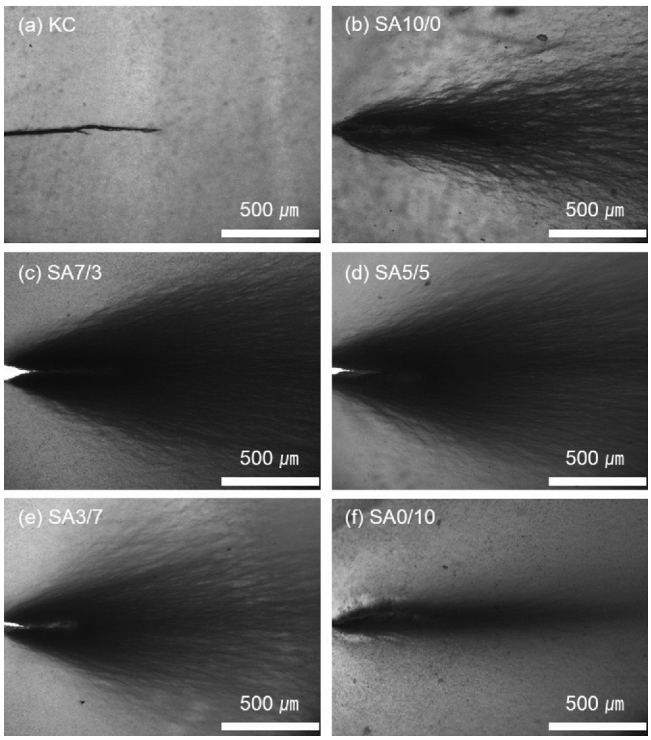

Figure 6. TOM images showing sub-surface damage zone of DN-4PB test specimens of PK/PC blends: (a) KC, (b) SA10/0, (c) SA7/3, (d) SA5/5, (e) SA3/7, and (f) SA0/10.

since the SEBS phase was separately dispersed in the PK matrix.

As shown in Figure 4(d), a notable enhancement of the impact strength was observed in the PK/PC/SEBS/PA6. In the PK/PC and PK/PC/SEBS, premature detachment of the PC particles occurred at the interface which led to a low impact strength. On the other hand, for the PK/PC/SEBS/PA6 blends, completely or incompletely encapsulated PC particles acted as stress concentrators to absorb impact energy in the matrix due to the improved interfacial adhesion. The PK/PC/(SEBS-*g*-MA/unSEBS)/PA6 blends showed a higher impact strength than the PK/PC/SEBS-*g*-MA/PA6 blend. When the ratio of SEBS-*g*-MA to unSEBS was 7/3, the impact strength was the highest, which was 60% higher than that of PK. The interfacial adhesion of SA7/3 was considered to be the most suitable level to mitigate impact energy. As the content of the unSEBS in the SEBS-*g*-MA/unSEBS mixture was increased by more than 30%, the impact strength decreased gradually.

3.4. Toughening mechanism

The impact-fracture surfaces reflecting the fracture process of the blends were examined. As shown in Figure 5(a), the fracture surface of KC exhibited two regions with a distinct boundary: a slow-crack-growth region next to the notch root and a fast-crack-growth region with feather-like markings. The surface of slow-crack-growth region was smooth without any markings under low magnification. In the region, the crack propagation was slow. In the fast-crack-growth region, a number of feather-like markings were generated by intersection of the main crack front with secondary cracks propagating from the flaws on different planes. The feather-like markings characteristic of brittle polymers indicate that the crack propagation progressed rapidly.[29] In the magnified image (Figure 5(b)), traces of particles being pulled out of the matrix during impact-fracture process were observed. For SA10/0, the distinction between the slow- and fast-crack-growth regions was less clear as the number of feather-like markings in the fast-crack growth region decreased. This was thought to be the result of the crack propagation rate being reduced by the crack deflection process. Crack deflection could have occurred by the PC particles which were located in the path of a propagating crack.[30] In Figure 5(d), it was confirmed that small PC particles were well dispersed in the PK matrix without detachment. Due to the complete encapsulation of PC by SEBS, high energy was required to initiate debonding. The fracture surface of SA7/3 was significantly different from the above two. As the feather-like markings disappeared, the distinction between slow- and fast-crack-growth regions became impossible. As shown in Figure 5(f), extensive debonding and deformation of the matrix appeared in SA7/3. The incomplete encapsulation of PC caused debonding at the interface. However, the debonding did not become large enough to cause a premature fracture due to the energy dissipation by the deformation of the SEBS. The void formation not only relaxed the triaxial stress but also induced shear yielding in the matrix by reducing the matrix ligament thickness.[31,32]

The observation of sub-surface damage zone around crack tip of the DN-4PB specimens was conducted to investigate the

toughening mechanisms of the blends. The damage zones appeared in the bright-field TOM images due to light scattering from crazes and voids generated during DN-4PB test (Figure 6). For KC, only a main crack existed at crack tip. The crazing capable of relaxing triaxial stress constraint did not occur because of the poor interfacial adhesion. As a result, the impact strength of KC was inevitably low. On the other hand, the TOM image of SA10/0 showed that a large damage zone appeared around the crack tip. The completely encapsulated PC particles served as stress concentrators to trigger crazing.[33] The damage zones of SA7/3 and SA5/5 were wider and more intense than that of SA10/0. The wide damage zones of these blends containing the incompletely encapsulated PC particles were due to the debonding and shear yielding. In the case of SA0/10 where the unSEBS and PC were dispersed separately in the matrix, the size of the damage zone was reduced again as the aforementioned effect of the toughening mechanisms disappeared.

4. Conclusions

The PK/PC blends were compatibilized by PA6 and mixtures of SEBS and MA-grafted SEBS, and the relation between the phase morphology and impact behavior was investigated. The phase morphology of the blends was dependent on the SEBS-*g*-MA/unSEBS ratio. Complete encapsulation of PC by SEBS was observed in the PK/PC/SEBS-*g*-MA/PA6 blend while the PK/PC/(SEBS-*g*-MA/unSEBS)/PA6 blends showed incomplete encapsulation of PC. When impact stress was applied, the incomplete encapsulation of PC caused debonding at the interface where SEBS was not placed. The debonding occurred in the PK/PC/(SEBS-*g*-MA/unSEBS)/PA6 blends appeared to relieve triaxial strain constraint, resulting in a more enhanced impact strength than that of the PK/PC/SEBS-*g*-MA/PA6 blends. The results suggested that the PK/PC/(SEBS-*g*-MA/unSEBS)/PA6 blend could be a suitable material for applications requiring mechanical properties with good balance of impact strength and stiffness.

Supporting information: Information is available regarding the phase morphology and interphase structure of PK/PC/unSEBS blend (S0/10). The materials are available *via* the Internet at http://www.springer.com/13233.

References

(1) M. A. Del Nobile, G. Mensitieri, L. Nicolais, A. Sommazzi, and F. Garbassi, *J. Appl. Polym. Sci.*, **50**, 1261 (1993).
(2) A. Sommazzi and F. Garbassi, *Prog. Polym. Sci.*, **22**, 1547 (1997).
(3) E. Marklund, U. W. Gedde, M. S. Hedenqvist, and G. Wiberg, *Polymer*, **42**, 3153 (2001).
(4) H. Unal, A. Mimaroglu, and T. Arda, *Appl. Surf. Sci.*, **252**, 8139 (2006).
(5) Y. Kim, J. W. Bae, C. S. Lee, S. H. Kim, H. Jung, and J. Y. Jho, *Macromol. Res.*, **23**, 971 (2015).
(6) W. C. J. Zuiderduin, D. P. N. Vlasveld, J. Huétink, and R. J. Gaymans, *Polymer*, **45**, 3765 (2004).
(7) W. P. Gergen and R. G. Lutz, US Patent 5,071,916 (1991).
(8) J. M. Machado and R. P. Gingrich, US Patent H1601 (1996).
(9) A. Asano, M. Nishioka, Y. Takahashi, A. Kato, S. Hikasa, H. Iwabuki, K. Nagata, H. Sato, T. Hasegawa, H. Sawabe, M. Arao, T. Suda, A. Isoda, M. Mukai, D. Ishikawa, and T. izumi, *Macromolecules*, **42**, 9506 (2009).
(10) W. P. Gergen, J. M. Machado, D. G. Waters, and R. P. Gingrich, US Patent 5,043,389 (1991).
(11) W. P. Gergen and W. W. C. Hart, US Patent 4,960,838 (1990).
(12) B.-B. Wang, L.-X. Wei, and G.-S. Hu, *J. Appl. Polym. Sci.*, **110**, 1344 (2008).
(13) A. N. Wilkinson, M. L. Clemens, and V. M. Harding, *Polymer*, **45**, 5239 (2004).
(14) Y. Zhou, W. Wang, R. Dou, L.-P. Li, B. Yin, and M.-B. Yang, *Polym. Eng. Sci.*, **53**, 1845 (2013).
(15) H.-M. Chen, X.-F. Wang, D. Liu, Y.-P. Wang, J.-H. Yang, Y. Wang, C.-L. Zhang, and Z.-W. Zhou, *RSC Adv.*, **4**, 40569 (2014).
(16) C. H. Lee, Y. M. Lee, H. K. Choi, S. Horiuchi, and T. Kitano, *Polymer*, **40**, 6321 (1999).
(17) Y.-T. Shieh, T.-N. Liao, and F.-C. Chang, *J. Appl. Polym. Sci.*, **79**, 2272 (2001).
(18) D. Sémeril, E. Passaglia, C. Bianchini, M. Davies, H. Miller, and F. Ciardelli, *Macromol. Mater. Eng.*, **288**, 475 (2003).
(19) B. Li, C. Wan, Y. Zhang, and J. Ji, *J. Appl. Polym. Sci.*, **115**, 3385 (2010).
(20) S. Horiuchi, N. Matchariyakul, K. Yase, T. Kitano, H. K. Choi, and Y. M. Lee, *Polymer*, **37**, 3065 (1996).
(21) T. S. Omonov, C. Harrats, and G. Groeninckx, *Polymer*, **46**, 12322 (2005).
(22) S.-K. Na, B.-G. Kong, C. Choi, M.-K. Jang, J.-W. Nah, and J.-G. Kim, *Macromol. Res.*, **13**, 88 (2005).
(23) S. De Vito, F. Ciardelli, G. Ruggeri, O. Chiantore, and A. Moro, *Polym. Int.*, **45**, 353 (1998).
(24) Y. Kim, C. S. Lee, S. Kim, H. Jung, and J. Y. Jho, *Macromol. Res.*, **23**, 965 (2015).
(25) X. Zhou, P. Zhang, X. Jiang, and G. Rao, *Vib. Spectrosc.*, **49**, 17 (2009).
(26) K. Faghihi and M. Shabanian, *Int. J. Polym. Mater.*, **60**, 505 (2011).
(27) K. H. Han, M. G. Jang, K. J. Juhn, C. Cho, and W. N. Kim, *Macromol. Res.*, **26**, 254 (2018).
(28) S. Horiuchi, N. Matchariyakul, K. Yase, T. Kitano, H. K. Choi, and Y. M. Lee, *Polymer*, **38**, 6317 (1997).
(29) Z.-Z, Yu, Y.-C. Ke, Y.-C. Ou, and G.-H. Hu, *J. Appl. Polym. Sci.*, **76**, 1285 (2000).
(30) K. T. Faber and A. G. Evans, *Acta Metall.*, **31**, 565 (1983).
(31) R. J. M. Borggreve, R. J. Gaymans, and H. M. Eichenwald, *Polymer*, **30**, 78 (1989).
(32) S.-C. Wong and Y.-W. Mai, *Polymer*, **41**, 5471 (2000).
(33) G.-X. Wei, H.-J. Sue, J. Chu, C. Huang, and K. Gong, *J. Mater. Sci.*, **35**, 555 (2000).